Location of seismicity: a migration based approach

S. Rentsch, S. Buske, S. Lüth, and S. A. Shapiro

email: *rentsch@geophysik.fu-berlin.de*

keywords: *Passive seismic monitoring, location, Gaussian beams*

ABSTRACT

We propose a new approach for precise location of seismic sources using a Gaussian beam type migration of multicomponent data. This approach requires only the preliminary picking of event time intervals and is much less sensitive to the picking precision than standard location procedures. Furthermore, this approach is characterised by a high degree of automation. The polarisation information of multicomponent data is used to perform initial-value ray tracing. By weighting the energy of the signal using Gaussian beams around these rays the stacking of energy is restricted to physically relevant regions only. Event locations correspond to regions of maximum energy in the resulting image. We show successful applications of the method to synthetic data examples with 20-30 per cent white noise and to real data of an hydraulic fracturing experiment.

INTRODUCTION

A precise location of seismic sources (i.e., attributing events to spatial coordinates of their hypocenter) is an important issue in a broad range of geophysical applications. This includes, e.g., earthquake seismology (Thurber and Rabinowitz, 2000) and seismicity based reservoir monitoring (Maxwell and Urbancic, 2001).

Several location procedures require identification of seismic phases and picking of P- and S-wave arrival times as well as determination of the velocity structure between the hypocenter and the seismic station. One method is to calculate predicted arrival times for the seismic stations and relate arrival time residuals to the hypocenter and its origin time. The calculation of the predicted arrival times is repeated until arrival time residuals are sufficiently small (Thurber and Rabinowitz, 2000). Furthermore, the circle method is often used for location of the hypocenter and the origin time. The difference between P- and S-wave arrival times for all receivers are used to calculate hemispheres of travel-distances. The hypocenter is assigned to the intersecting region of these hemispheres (Lay and Wallace, 1995). These standard location procedures are characterised by a strong dependence on event picking accuracy and a low degree of automation. Manual picking in the case of large data sets makes the process of location very slow, expensive and not practicable.

In contrast, we propose an automated location procedure that takes into account the full elastic wavefield of multicomponent data. Our method is based on the principles of wave field back-propagation and uses a Gaussian beam type migration in order to image seismic sources.

CONCEPT OF THE LOCATION PROCEDURE

The first step in our procedure is to find an event within the recorded data stream. This can be done by an approximate automatic detection algorithm (e.g., Baer and Kradolfer, 1987). Then a time interval around this event is selected, which contains at least the full waveform of the event. By analysing the three components of this signal we obtain the polarisation for each time sample. Then, initial-value ray tracing is performed using this polarisation information as the starting direction of the ray (see Figure 1(a)). In order to obtain the image value for an arbitrary grid point $P(x, y, z)$ a Gaussian beam type back-propagation is performed. This means that the energy $E(t)$ of the signal is weighted mainly with a Gaussian beam type

factor (Cerveny, 2001) and a summation of all weighted energies over all receivers is done to construct the image:

$$M(x,y,z) = \sum_{Receiver} \int_{t_1}^{t_2} E_{Receiver}(t) \cdot \exp(-(r^2)/(b^2))dt. \quad (1)$$

The times t_1 and t_2 correspond to the range of the previously picked time interval. The shape of the Gaussian beam is controlled by the beam width b and the perpendicular distance r of the grid point $P(x,y,z)$ from the corresponding central ray (see Fig. 1(a)).

Significant energy-values are concentrated within the beam width. Outside the beam width these values rapidly decrease due to the weighting of the energy with a Gaussian beam type factor (exponential function in equation 1). Hence, the weighting restricts the back-propagation along the rays as shown in Fig. 1(b) as shaded areas. Summation over all receivers leads to regions of distinct stacked energy.

Thus, the region in the final image $M(x,y,z)$ with maximum stacked energy is assumed to represent the hypocenter of the event (see Fig. 1(b)).

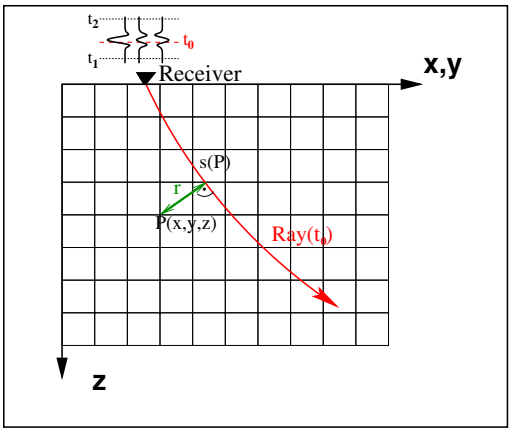

(a) Initial-value ray tracing is performed for the time sample t_0. The perpendicular distance r from a grid point $P(x,y,z)$ to the ray and the ray parameter $s(P)$ is needed for amplitude weighting.

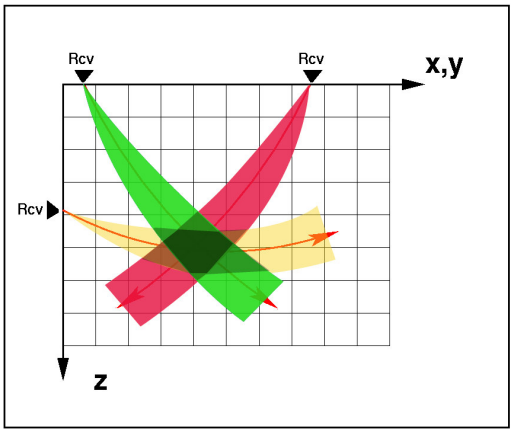

(b) Scheme of an image obtained by initial-value ray tracing, energy weighting and summation over 3 receivers for a time sample t_0. The region with maximum energy is considered to be the hypocenter of the event.

Figure 1: Concept of the location method.

In order to take into account the uncertainty of location with increasing depth the raylength $s(P)$ (see Fig. 1(a) and Fig. 1(b)) has to control the width b of the Gaussian beam. We define the width of the Gaussian beam depending on the raylength in terms of the Fresnel radius. This physically means that the beamwidth increases with increasing raylength.

APPLICATION TO SYNTHETIC DATA

The approach was applied to 3D isotropic and homogeneous synthetic models. As representative examples the results of two data sets are presented. We assigned a constant P-wave velocity of 6 km/s to the model with dimensions 2000m x 2000m x 2500m. The event was assumed as an exploding point source at x=1000m, y=700m and z=1000m. The recording network of the first example consisted of 20 arbitrarily distributed surface stations (see Fig. 2(a)). Such a receiver geometry was used at the German Continental Deep Drilling Project for monitoring fluid induced microseismicity (Baisch et al., 2002). The three component data with 20 per cent white noise computed for this model are shown in Fig. 2(b).

The full traces of all 20 surface stations were processed as described above using a constant image grid spacing of 50m. The result is shown in Fig. 3(a) for a slice at y=700m. High energy is focusing in the center of the image and marks the location of the hypocenter of the event. In order to get a better impression of

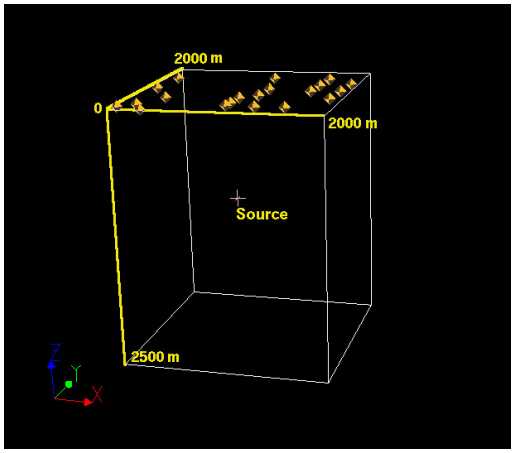

(a) A 3D isotropic and homogeneous model with an exploding point at x=1000m, y=700m and z=1000m. The recording network consists of 20 randomly distributed surface stations (orange diamonds)

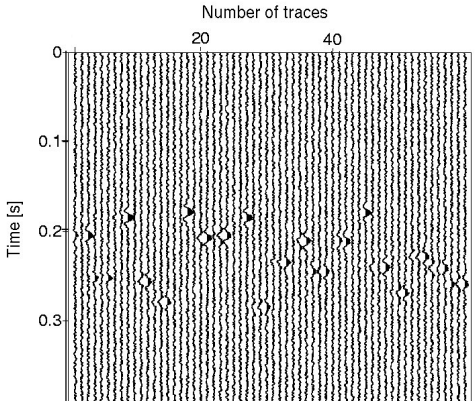

(b) The three component data with 20 per cent white noise computed for the 20 surface stations.

Figure 2: First synthetic data example: (a) receiver geometry and (b) the corresponding traces.

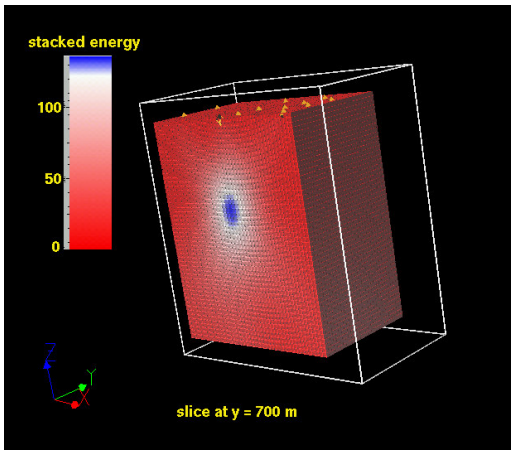

(a) Image at a slice y=700m. Colours represent values of stacked energy. Red colours correspond to small values and blue colours in the center of this image to large ones.

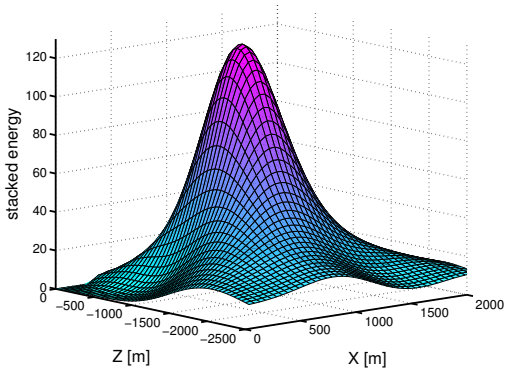

(b) Distribution of stacked energy at the displayed slice of Fig. 3(a) with maximum amplitude at x=1000m, y=700m and z=1000m.

Figure 3: Resulting image of the synthetic data example shown in Fig. 2(b) at slice y=700m.

the focus of high stacked energy for the slice y=700m the distribution of energy is shown in more detail in Figure 3(b). Energy values rapidly decay away from the maximum. This decay gives a qualitative estimate of the location uncertainty which means the stronger the decay the smaller is the uncertainty. For the presented example we obtain the coordinates of the maximum energy at x=1000m, y=700m and z=1000m which corresponds to the true event coordinates of the model.

For the second example we use a recording network of 20 surface stations with a constant interval of 100m. Recording geometries like receiver strings are often used for monitoring of hydraulic-fracturing experiments (e.g., Urbancic et al., 1999). White noise up to 30 per cent was added to the three component data. The resulting image for a slice at x=1000m is shown in Figure 4(a). Again, the region of high stacked energy is considered as the event location. The elliptic shape of the region is caused by the receiver geometry of a single receiver string. The distribution of stacked energy at slice x=1000m is shown in Figure 4(b). Also for this example we obtain the coordinates of the grid point with the maximum energy at x=1000m, y=700m and z=1000m which corresponds to the true event coordinates of the model.

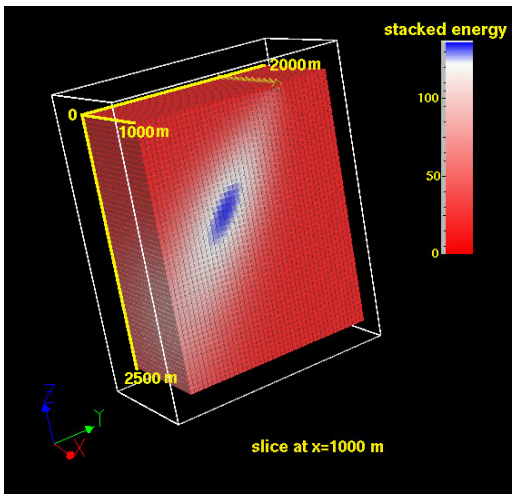

(a) Image at slice x=1000m. Colours represent values of stacked energy as described in Figure 3(a). The region of high stacked energy (elliptic blue area in the center of this image) marks the hypocenter of the event.

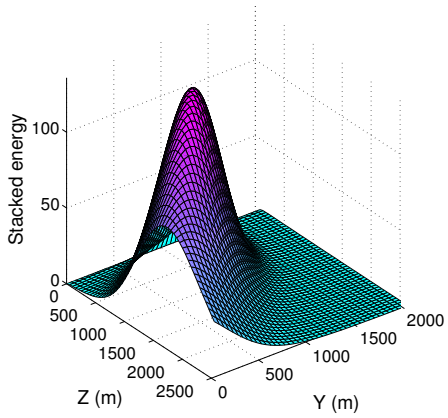

(b) Distribution of stacked energy at the displayed slice of Figure 4(a) with maximum energy at x=1000m, y=700m and z=-1000m.

Figure 4: Resulting image for the second synthetic model.

Two different receiver geometries and noise levels up to 30 per cent were used to compute synthetic data. For both presented examples the hypocenter of the event was located sufficiently well. The uncertainty of location depends mainly on the signal-to-noise ratio because noise in the data affects the polarisation information which is used to perform the initial-value ray tracing. Also, perceptible discrepancies of the velocity model affect the ray tracing. Thus the location uncertainty also depends on the accuracy of the velocity model. The geometry of receivers, the chosen grid dimension for the migration and the width of the Gaussian beam also influence the location accuracy, but tests on synthetic data have shown that these influences are less critical.

CASE STUDY

During a hydraulic fracturing experiment at the Cotton Valley field (East Texas, USA) more than 900 microseismic events were recorded using two monitoring wells (CGU 21-9 and CGU 22-9). These monitoring wells were located approximately 400 m to the East and Northeast of the treatment well (GCU 21-10). The sensor array consisted of 48 three component receivers at 15 m spacing in each monitoring well (Urbancic et al., 1999). Unfortunately, it was not possible to use all 96 receivers to perform our migration method for

event location. Some receivers have shown broken down components or were completely broken down. Other receivers have shown significant differences in the mean noise amplitudes on their three components. This can be caused by differences in the sensitivity or coupling and disturbs the polarisation. Hence, in this study only sensors displaying equal signal-to-noise levels on every component (4 sensors in CGU 21-9 and 16 in CGU 22-9) were used to locate the events.

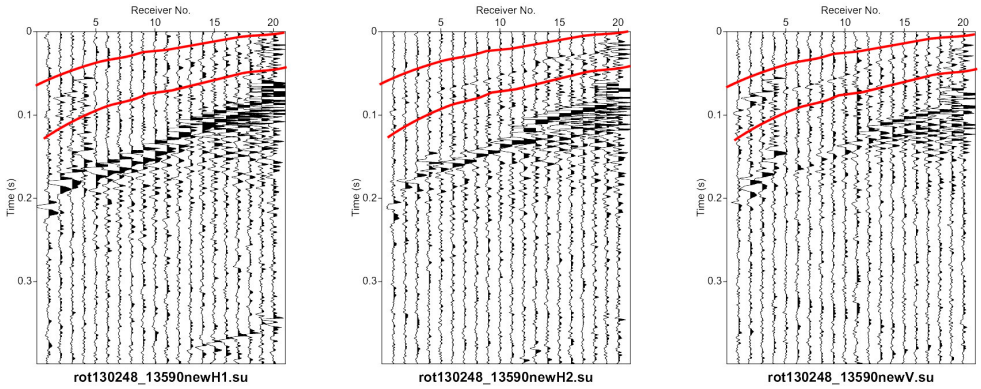

Figure 5: Traces of a microseismic event for 20 selected receivers (4 sensors in CGU 21-9 and 16 in CGU 22-9). Horizontal components are rotated into the geographical coordinate system. The waveforms around the P-wave onset (waveforms within the red marked interval) were used for migration.

Traces of these 20 receivers were rotated into the geographical coordinate system (see Figure 5 as an example of one microseismic event) and waveforms around the P-wave onset were selected (see red marked interval in Figure 5). The corresponding image for this event is shown in Figure 6. High energy (red and white colors) marks the hypocenter of event. The region of high energy has an elliptic shape like the result for the second synthetic example. Again this is caused by the receiver geometry because all rays are traced approximately in the same direction.

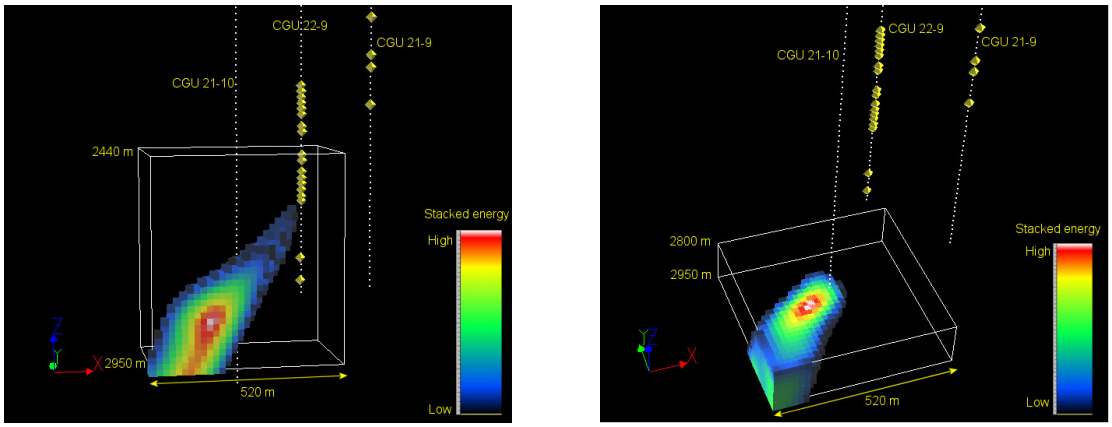

(a) Image slice 50 m south of the treatment well.

(b) View from above at depth of 2800 m.

Figure 6: Resulting image for the event shown in Figure 5. Colors represent values of stacked energy. Yellow diamonds mark the used receivers. The region with maximum energy marks the hypocenter of this microseismic event.

We give a comparison of different event location results in Figure 7. Green stars correspond to event

locations obtained by the application of our migration algorithm. Red and blue stars belong to event locations using P- and S-wave arrival times (Rutledge et al., 2004, 1998). Our event locations show a very good agreement with the results of the other methods. Deviations of the locations might be due to different velocity models.

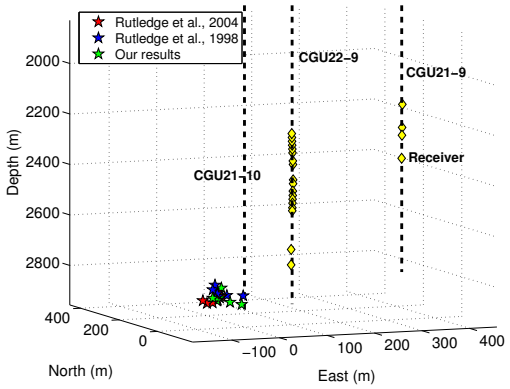

(a) 3D view of location results from Southwest. Wells are shown as black dashed dotted lines. Yellow diamonds mark receivers used to obtain our results.

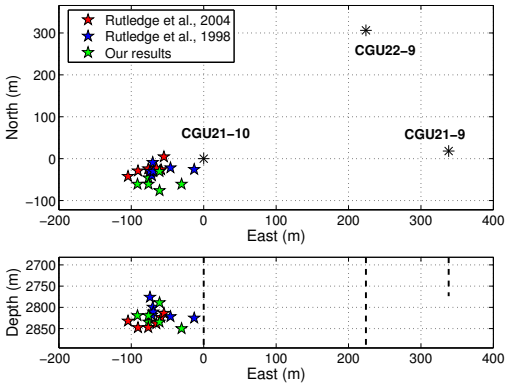

(b) Map and depth view of hypocenters.

Figure 7: Comparison of event locations obtained by different location methods. Blue marked locations belong to initial locations from Rutledge et al. (1998) and red marked events to relocated hypocenters from Rutledge et al. (2004). Locations colored in green were obtained using our approach.

CONCLUSIONS

A new method for location of seismic sources using multicomponent data is presented. The concept is based on the principles of wave field back-propagation and uses a Gaussian beam type migration. By using Gaussian beams for amplitude weighting the migration operator is restricted to the width of a Gaussian beam around each ray, which represents the physically relevant region of the wavefield. The hypocenter of the event is assigned to the region with maximum amplitude in the final image. Successful applications of the approach are presented on two synthetic data example with different noise levels and different receiver geometries. The approach was also successfully applied to real data from the Cotton Valley hydraulic fracture experiment. The uncertainty of location is mainly affected by the signal-to-noise ratio and less affected by the geometry of receivers, the chosen grid dimension for the migration and the width of the Gaussian beam.

The presented approach is characterised by a high degree of automation because time consuming manual picking of arrival times is not necessary. In the next steps we will include S-waves into the location procedure.

ACKNOWLEDGEMENTS

This work was kindly supported by the sponsors of the *Wave Inversion Technology (WIT) Consortium*, Karlsruhe, Germany.

REFERENCES

Baer, M. and Kradolfer, U. (1987). An automatic phase picker for local and teleseismic events. *Bull. Seismol. Soc. Am.*, 77:1437–1445.

Baisch, S., Bohnhoff, M., Ceranna, L., Tu, Y., and Harjes, H.-P. (2002). Probing the crust to 9 km depth:

Fluid injection experiments and induced seismicity at the KTB superdeep drilling hole, Germany. *BSSA*, 92:2369–2380.

Cerveny, V. (2001). *Seismic Ray Theory*. Cambridge Univ. Press, 713 pages.

Lay, T. and Wallace, T. C. (1995). *Modern global seismology*. Academic Press, 521 pages.

Maxwell, S. and Urbancic, T. (2001). The role of passive microseismic monitoring in the instrumented oil field. *The Leading Edge*, pages 636–639.

Rutledge, J. T., Phillips, W. S., House, L., and Zinno, R. (1998). Microseismic mapping of a Cotton Valley hydraulic fracture using decimated douwnhole arrays. *Soc. Explor. Geophys., 68nd Ann. Internat. Mtg., Expanded Abstracts*, pages 338–341.

Rutledge, J. T., Phillips, W. S., and Mayerhofer, M. J. (2004). Faulting induced by forced fluid injection and fluid flow forced by faulting: An interpretation of hydraulic-fracture microseismicity, Carthage Cotton Valley gas field. *Bull. Seism. Soc. Am.*, 94:1817–1830.

Thurber, H. C. and Rabinowitz, N. (2000). *Advances in Seismic Event Location*. Kluwer Academic Publishers, 267 pages.

Urbancic, T. I., Shumila, V., Rutledge, J. T., and Zinno, R. J. (1999). Determining hydraulic fracture behavior using microseismicity. *Vail Rocks '99, 37th US Rock Mechanics Symposium, Vail, Colorado*, pages 991–996.